Horizontal Tailplane Subjected to Impact Loading

M. Hörmann[a], U. Stelzmann[a], M.A. McCarthy[b], J.R. Xiao[c]

[a] *CAD-FEM GmbH, Grafing/Munich, Germany*
[b] *Department of Mechanical and Aeronautical Engineering, University of Limerick, Limerick, Ireland*
[c] *Center for Composite Materials, University of Delaware, Newark, DE 19716, USA*

Abstract

The European Union Research Programme CRAHVI (CRashworthiness of Aircraft for High Velocity Impact) is concerned with the high velocity impact of aircraft due to flying objects, e.g. bird, hailstone, tyre and engine debris as well as concerned with survivable crash landings on different surfaces, e.g. rigid inclined surfaces (slopes) and water with different sea states. The simulation is naturaly a complex task due to the high number of variables involved. Such variables include material characteristics of the impacted media, impactors and surfaces at high strain rate, and the interaction between the aircraft structure and the impactors or surfaces. But with the increase of software and hardware computing power, it is now becoming more realistic to predict the behaviour of aircraft structures subjected to high velocity impact scenarios.

Within the CRAHVI-Programme finite element models of a clamped horizontal tailplane (HTP) in an airliner are developed, which are subjected to impact loading with different impactor models. The HTP model composed of advanced composite material has been delivered by the University of Limerick [2],[3] whereas the HTP model representing metallic material was provided by the University of Patras [4]. Based on these models, the National Aerospace Laboratory NLR delivered an input file for the impact of a Lagrangian bird model on the HTP [8]. All files have been provided in form of PAM-CRASH input.

*It was the task of CAD-FEM to transfer those models into LS-DYNA input files, whereby special attention must be paid on a proper translation of the corresponding material models and the automatic generation of spotwelds. In case of the used composite bi-phase material the *MAT_LAMINATED_COMPOSITE_FABRIC model of LS-DYNA [11] is used. Based on those translated input files selective simulations for the composite and metallic structure are performed including bird strike on the leading edge (LE) of the HTP. For the bird strike simulation a Lagrangian as well as an ALE formulation is used. Additionally LS-OPT [10] was used in the Lagrangian bird strike simulation performing a thickness optimization of the LE. The optimization goal for bird strike is shortly speaking a non-rupture of the LE.*

The current contribution presents simulation results of rigid pole impact on composite HTP model, bird strike within Lagrangian formulation on metallic HTP model and bird strike within ALE formulation on metallic HTP model. Moreover the results are compared with other numerical results available within the CRAHVI-Programme. Additionally optimization results of the LE obtained from LS-OPT in combination with LS-DYNA are shown, which fulfill the desired optimization criterion of a non-ruptured leading edge.

Acknowledgements

CRAHVI – Crashworthiness of Aircraft for High Velocity Impact is a RTD project partially funded by the European Union under the European Commission GROWTH programme, Key Action: New Perspectives in Aeronautics, Contract No. GRD1-2000-25242.

Introduction

In the European Union Research Programme CRAHVI (CRashworthiness of Aircraft for High Velocity Impact) finite element models were developed which are suitable to be used for deterministic and stochastic simulations in subsequent tasks. The basic structure is a clamped horizontal tailplane (HTP) of an airliner. The HTP is subjected to impact loading with different impactor models developed in work package 1 of the CRAHVI-Programme. It was the task of CAD-FEM in Deliverable 3.1.9 [9] to transfer those FE-models into LS-DYNA and to perform selective deterministic simulations for the composite and metallic structures including bird strike. For the latter one a Lagrangian as well as an Arbitrary-Lagrangian-Eulerian (ALE) approach was used. For the HTP made of composites the composite material model *MAT_LAMINATED_COMPOSITE_FABRIC was used, which seems to be an appropriate model compared to that used in PAM-CRASH. The finite element analysis has been performed using LS-DYNA (Version 970) [11].

Simulation results of rigid pole impact on composite HTP model, bird strike within Lagrangian formulation on metallic HTP model and bird strike within ALE formulation on metallic HTP model are presented and compared with previous results of the CRAHVI-Programme.

Additionally the contribution covers optimization results of the leading edge with respect to bird strike using the Lagrangian approach. The optimization goal is formulated as follows: ***Determine the thickness of the leading edge metal sheet, which minimizes the mass subjected to failure constraints with an upper boundary.*** The equivalent plastic strain at selected integration points is used as failure constraints. The optimization procedure leads to an optimized leading shell thickness of approximately 3.63 mm compared to the original value of 3.00 mm. With this specific leading edge shell thickness bird strike does not lead to a rupture of the leading edge, i.e. the structural integrity is not lost for the optimized leading edge.

Rigid Pole Impact

The finite element model of the horizontal tailplane (HTP) of an airliner was delivered by the University of Limerick as PAM-CRASH input file ([2] and [3]). The finite element model consists of a refined mesh for the composite structure based on a checkstress mesh provided from EADS-CASA. The composite tailplane structure is composed of two main parts, the leading edge (LE) and the box. The composite materials are retained with metallic parts, the LE nose (titanium alloy) and the LE spars (aluminium alloy). Material properties are provided by EADS-CASA.

The model contains approximately 26400 nodes, 1900 solid elements, 20600 shell elements and 1700 beam elements defined in the input deck. The basic units used are:

- length : m
- mass : kg
- force : N
- time : s

The HTP moves in negative x-direction with an initial velocity of 39 m/s and hits a rigid circular pole fixed in space, see Figure 1. Additionally node 5501040 is depicted in Figure 1, which will be used later for reference.

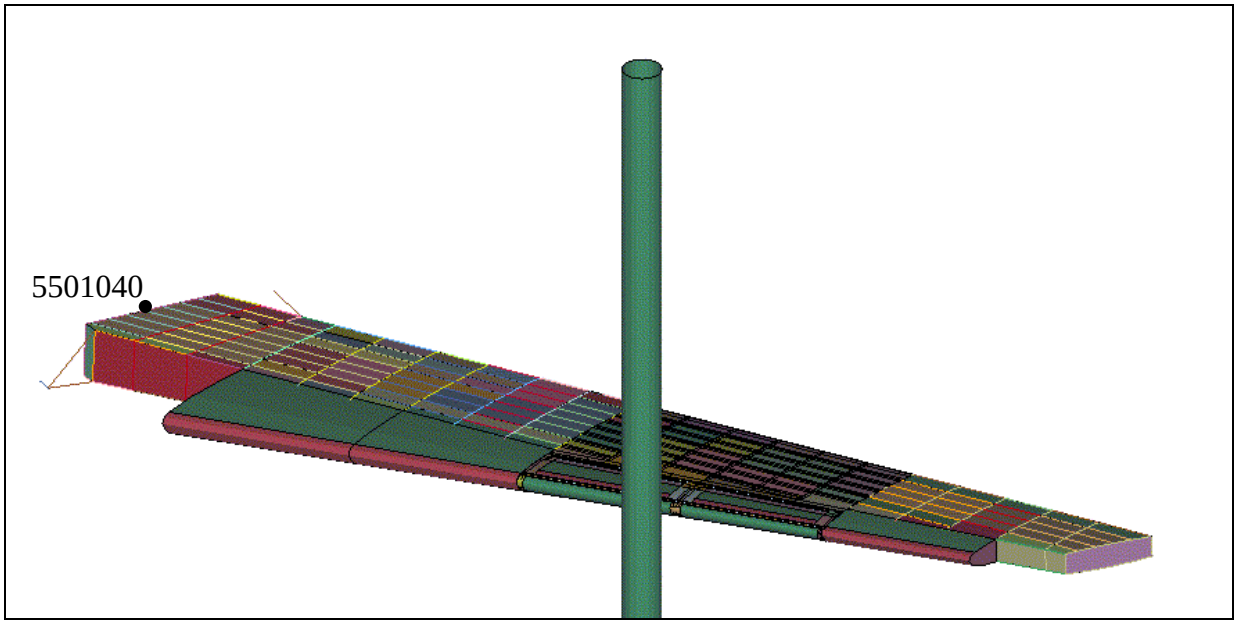

Figure 1: Finite element model of the composite HTP structure

The transformation of the HTP-model from PAM-CRASH to LS-DYNA input data has been performed using a Fortran-based conversion program. All mesh data and most common material and contact definitions are automatically translated. Special attention must be paid on the proper selection of the used material model for composites as well as on the proper generation of multilayered spotwelds.

Composite Material Model in LS-DYNA

Material model 130 in PAM-CRASH describes in combination with a ply definition a multi-layer and multi-material shell model. The material model is based on a unidirectional bi-phase material composed of fiber and matrix material properties taking the different tensile and compression behavior of both components into account.

An appropriate material model for orthotropic nonlinear material behavior in LS-DYNA is among others the *MAT_LAMINATED_COMPOSITE_FABRIC material model (#58), see [11]. It is based on a continuum damage mechanics approach introducing three independent damage variables ($0 \leq \omega_{ij} \leq 1$) in the relation of effective and nominal stresses $\hat{\sigma}$ and σ:

$$\hat{\sigma} = \begin{bmatrix} \hat{\sigma}_{aa} \\ \hat{\sigma}_{bb} \\ \hat{\sigma}_{ab} \end{bmatrix} = \begin{bmatrix} \frac{1}{1-\omega_{11}} & 0 & 0 \\ 0 & \frac{1}{1-\omega_{22}} & 0 \\ 0 & 0 & \frac{1}{1-\omega_{12}} \end{bmatrix} \begin{bmatrix} \sigma_{aa} \\ \sigma_{bb} \\ \sigma_{ab} \end{bmatrix}$$

Consequently the constitutive equation is also influenced and will continuously degrade in case of damage occurrence ($\omega_{ij} > 0$):

$$C_{ed}(\omega) = \frac{1}{D}\begin{bmatrix} (1-\omega_{11})E_p & (1-\omega_{11})(1-\omega_{22})\upsilon_{ba}E_n & 0 \\ (1-\omega_{11})(1-\omega_{22})\upsilon_{ab}E_p & (1-\omega_{22})E_n & 0 \\ 0 & 0 & D(1-\omega_{12})G \end{bmatrix}$$

with

$$D = 1 - (1-\omega_{11})(1-\omega_{22})\upsilon_{ab}\upsilon_{ba}$$

The damage variables describe failure in fiber direction ω_{11}, failure perpendicular to the fiber direction ω_{22} and inplane shear failure ω_{12}. Undamaged material corresponds to ω_{ij} =0; complete failure corresponds to ω_{ij} =1.

Different failure surfaces (*fs*) can be used (see Figure 2), depending on the type of used fiber-reinforced composite, i.e. unidirectional-reinforced or fabric-reinforced composite.

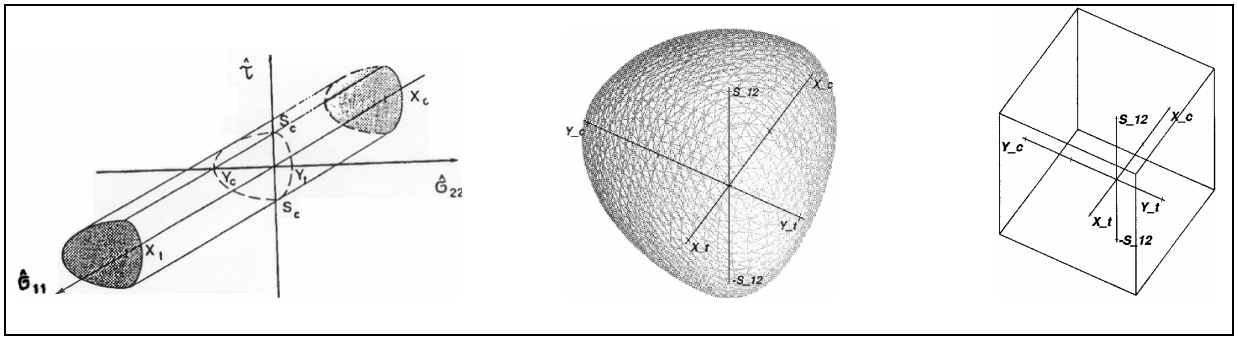

Figure 2: Available failure surfaces for LS-DYNA material model 58

The failure criteria are mainly based on the well-known Hashin direct mode criteria. Optional residual strength properties can be set in and perpendicular to the fiber direction as well as for inplane shear (*slimt1, slimc1, slimt2, slimc2, slims*). For woven fabrics a special treatment of the inplane shear stress-strain behavior can be used additionally (*tau1, gamma1*). Failure respectively eroding of the elements was defined by a failure eroding strain *erods*. The element elimination is slightly different from the PAM-CRASH model. For LS-DYNA layer elimination and element elimination are considered separately. In order to trigger the failure propagation a crash-front algorithm could be used (*soft*). Hereby the strength properties of elements in the vicinity of eroded elements are reduced, which describes a predamaging in the region ahead of the crack front. Evolution of damage (fast, delayed) can be optionally influenced by parameters *e11c, e11t, e22c, e22t* and *gms*. For a detailed description the reader is referred to [11].

Simulation Results: Rigid Pole Impact on Composite HTP Model

Figure 3 shows the perspective view of the rigid pole impact on the composite HTP model at two different time steps (rigid pole not shown). The HTP moves with an initial speed of 39 m/s, while the pole is fixed in space.

One might observe slivering and severe damage of the HTP leading to a complete cut through the HTP at final state, see Figure 5.

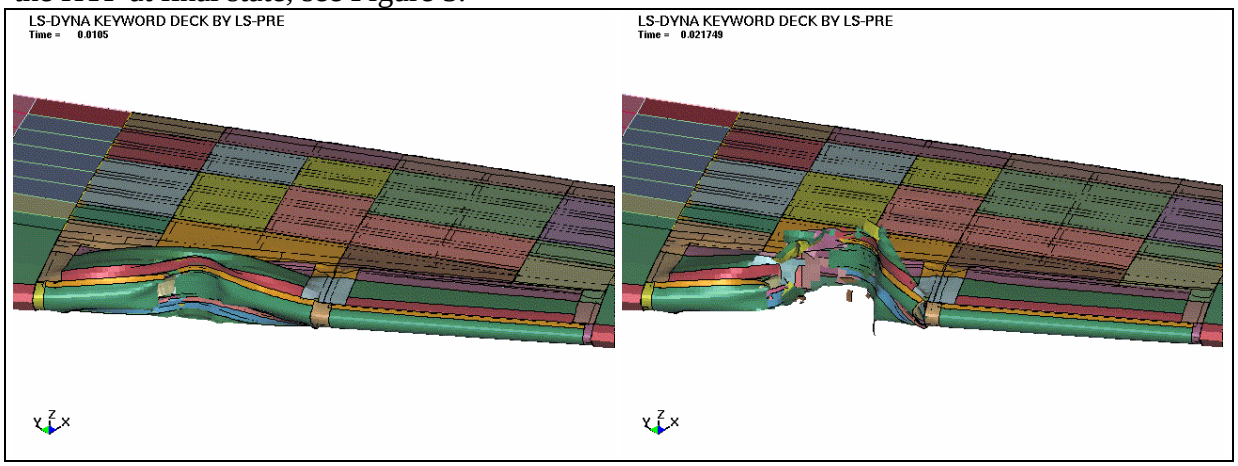

Figure 3: Perspective view of rigid pole impact on composite model

The leading edge is already highly deformed and has transferred a certain amount of kinetic energy into internal energy. The honeycomb material fails due to severe element deformations and consequently the solid elements are deleted, see Figure 4.

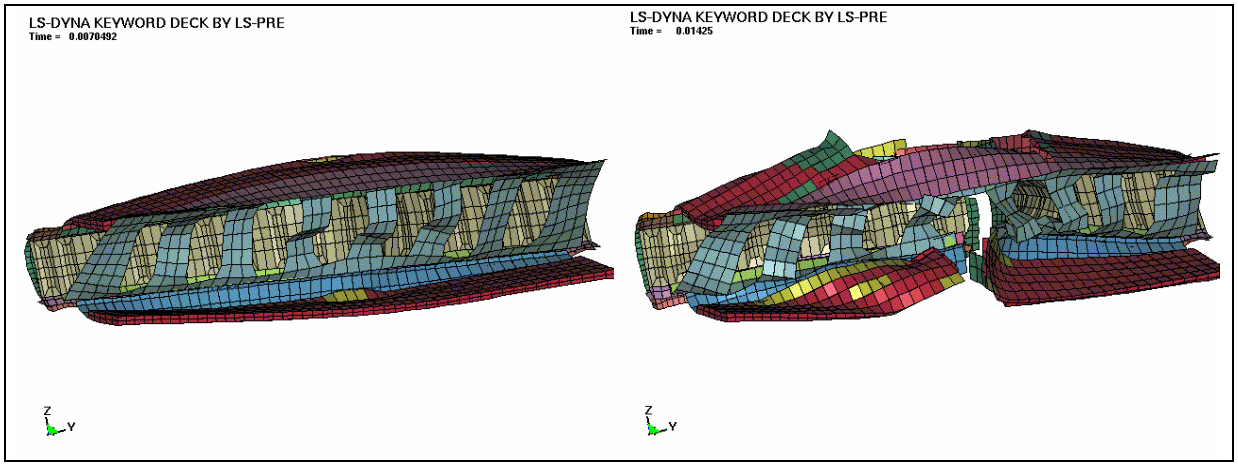

Figure 4: Interior view of the leading edge

Figure 5 depicts a comparison of PAM-CRASH and LS-DYNA deformation results. The state of failure at three specific times is shown as top view. According to Deliverable 3.1.7 [5] the first state at 7.3 ms is roughly the moment when the rigid pole hits the honeycomb, while the second state at 22 ms is when the impactor passes through the front spar. The final state in the composite model is the moment when the contact force became zero, i.e. when the impactor broke through the rear spar of the HTP.

The PAM-CRASH and LS-DYNA failure scenarios agree qualitatively very well but the time line of the LS-DYNA result seems to be slightly shorter. This means the cutting of the pole through the HTP is marginally faster in LS-DYNA than in PAM-CRASH. The pole needs approximately 92 ms to pass through the HTP. The LS-DYNA result therefore shows a slightly

softer behavior or the composite failure/erosion material model produces an earlier failure. Comparison to test results would be interested but are not available.

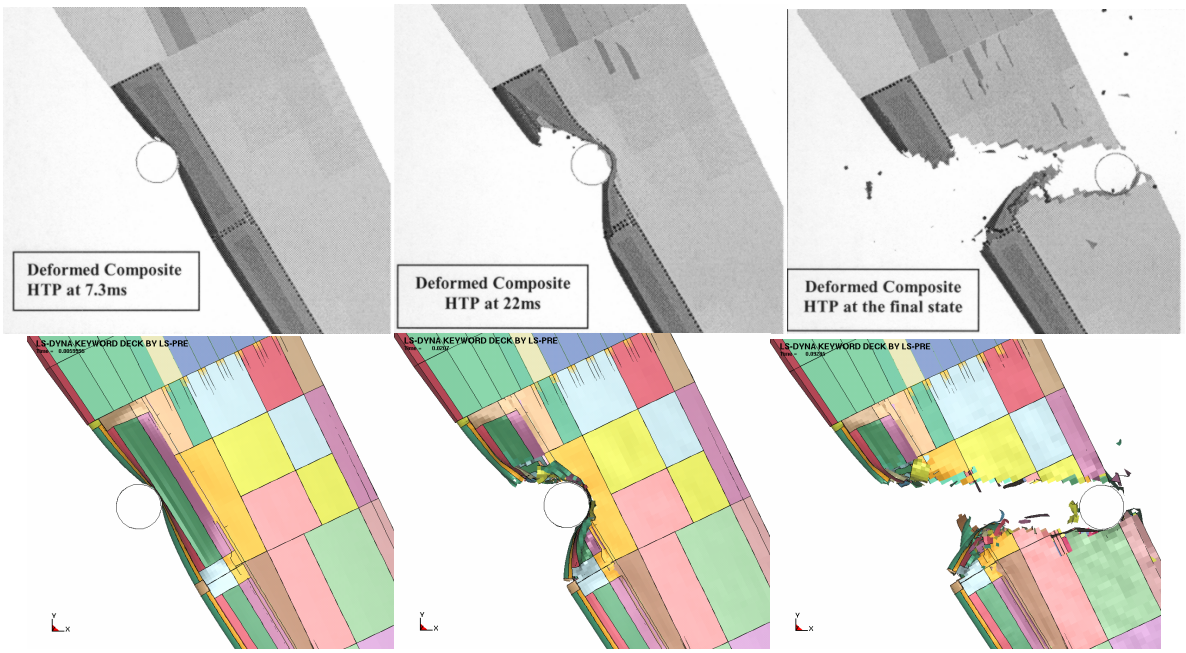

Figure 5: Comparison of failure scenario for PAM-CRASH [5] and LS-DYNA results

Figure 6 shows the comparison of the energy-time relationship for both simulation results. For the PAM-CRASH results a non-physical, jump-like increase in total energy is reported in Deliverable 3.1.7 [5]. Contrarily to those results the increase in total energy for LS-DYNA appears not suddenly but more gradually with stagnation at the end. The increase in total energy is approximately 25% for LS-DYNA and about 37% for PAM-CRASH. Moreover the intersection point of internal and kinetic energy appears not only at the same energy niveau but also at approximately the same time. No filtering option has been used for the LS-DYNA energy curves.

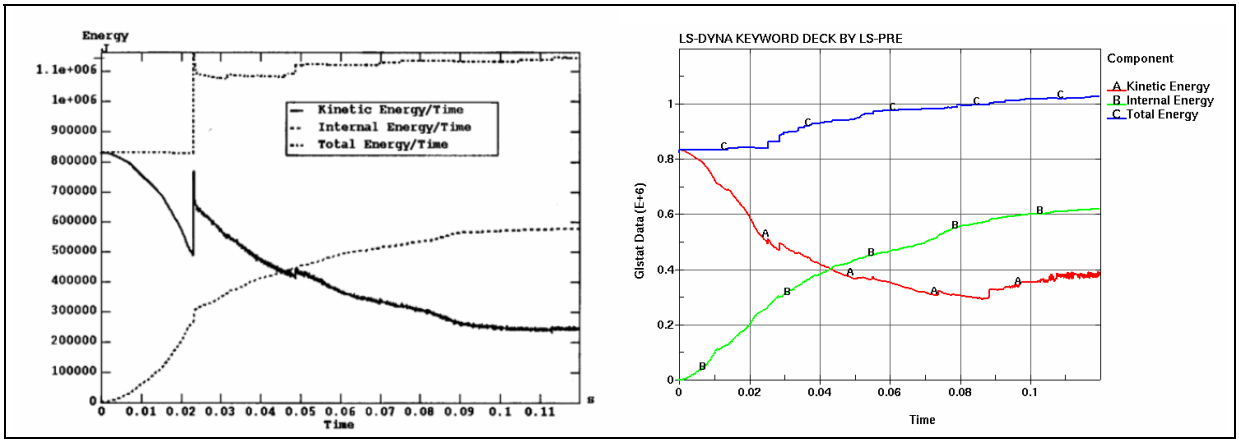

Figure 6: Comparison of energy vs. time for PAM-CRASH [5] and LS-DYNA results

Mass scaling has been used for the LS-DYNA simulation. Consequently it is important to check the total mass increase, see Figure 7a. Up to a time of 110 ms the total mass increase is insignificant and increases thereafter to a value of 0.1%, which is still negligible.

Figure 7b depicts the resultant velocity of node 5501040 vs. time for PAM-CRASH and LS-DYNA results. The location of point 5501040 is depicted in Figure 1. The agreement is up to the time 80 ms remarkable good but thereafter the results deviate from each other. The reason is, that the cutting through the HTP of the rigid pole is slightly faster in LS-DYNA than in PAM-CRASH, i.e. the PAM-CRASH result seems to be too stiff or the composite failure/erosion material model produces failure at later state. At time 92 ms the pole broke already through the rear spar leading to an almost constant resultant velocity.

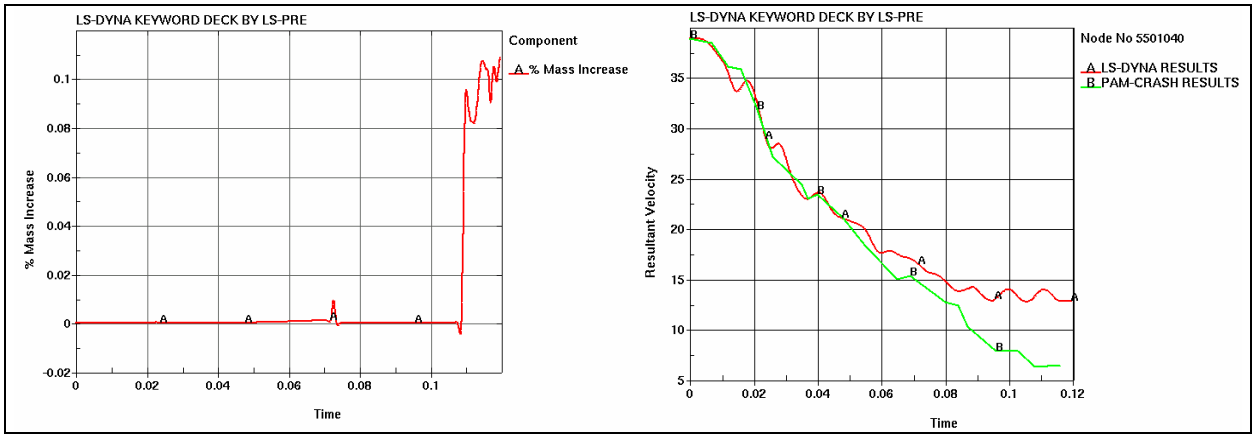

Figure 7: Total mass increase and resultant velocity of node 5501040 vs. time

Figure 8 depicts the relationship of resultant contact force vs. resultant displacement of node 5501040. The first peak at displacement u=0.37 and contact force F=0.72 does not fit very well to PAM-CRASH result (u=0.38, F=0.38). Although this first peak is obtained at approximately the same displacement it significantly differs in the resultant contact force. On the other hand the second peak at displacement u= 0.78 and contact force F=0.91 agrees very well with the PAM-CRASH result (u=0.77, F=0.93). Additionally the third peak at displacement u=2.0 is also well captured.

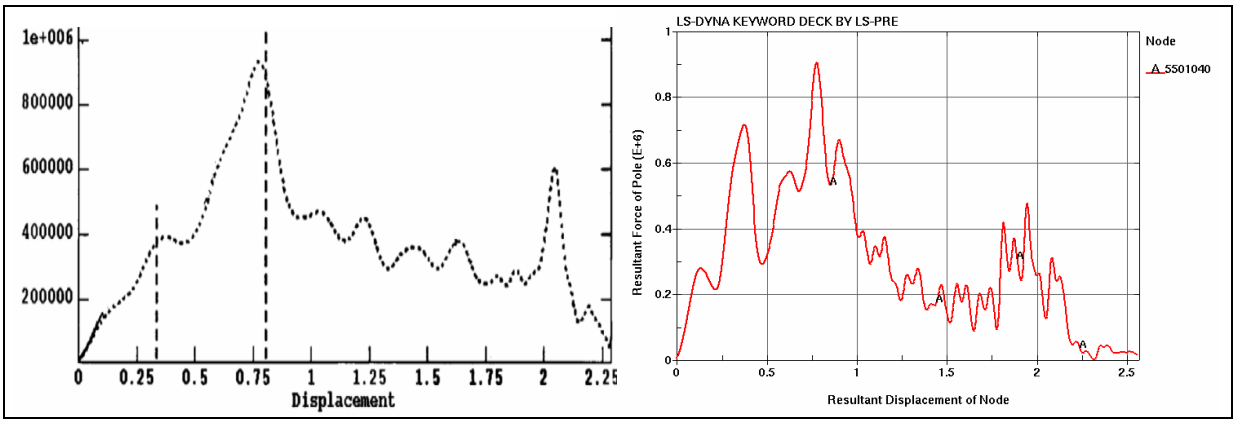

Figure 8: Contact force vs. displacement of node 5501040 for PAM-CRASH [5] and LS-DYNA

Bird Strike (Lagrange Formulation) on Metallic HTP Model

In subtask 3.1.5 of the CRAHVI European Union Research Programme, the National Aerospace Laboratory NLR has performed the simulation of a bird strike on the HTP. The Lagrangian FE bird model (D1.4.3) [6] is delivered by Airbus UK.

The following geometry data for the bird model is given:

- r = 0.057 m - h = 0.114 m
- l = 0.228 m - mass density = 934 kg/m^3

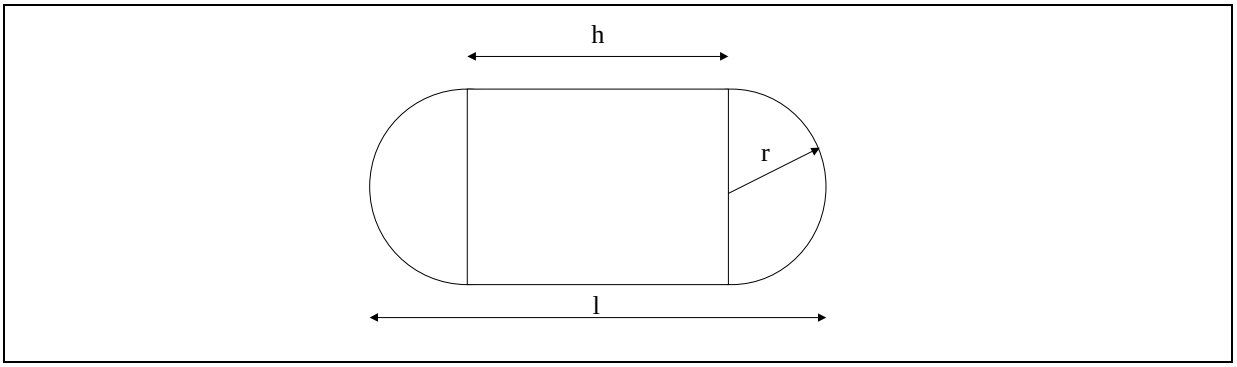

Figure 9: Geometry of the bird impactor model

For the material behavior under consideration an elastic-plastic hydrodynamic solid material (material type 7) in combination with a linear polynomial equation of state has been chosen in the PAM-CRASH model. The following material data is used:

- G = 2.0 GPa - C0 = 0.0 - C1=0.0
- σ_{yield} = 0.02 MPa - C2 = 0.0 - C3= 2.93E10 GPa

For the simulation with LS-DYNA material type 10 (*MAT_ELASTIC_PLASTIC_HYDRO) in combination with a linear polynomial equation of state to describe the increasing pressure within the bird is applied, see Table 1.

```
*MAT_ELASTIC_PLASTIC_HYDRO
$#     mid        ro         g      sigy        eh        pc        fs
  55420416  934.0000 1.000e+06 2.000e+04  1000.000       0.0       0.0
       0.0       0.0       0.0       0.0       0.0       0.0       0.0       0.0
       0.0       0.0       0.0       0.0       0.0       0.0       0.0       0.0
       0.0       0.0       0.0       0.0       0.0       0.0       0.0       0.0
       0.0       0.0       0.0       0.0       0.0       0.0       0.0       0.0
$
*EOS_LINEAR_POLYNOMIAL
$#   eosid        c0        c1        c2        c3        c4        c5        c6
  55420416       0.0       0.0       0.0 2.930e+10       0.0       0.0       0.0
       0.0       0.0
```

Table 1: Elasto-plastic hydrodynamic material model and equation of state

The default linear bulk viscosity 0.06 and the quadratic bulk viscosity 1.2 for PAM-CRASH are nearly the default values for LS-DYNA. The modification of these values to 0.01 and 0.1, which has been done in the NLR simulation, has been applied for the LS-DYNA input as well. Three different velocities (100, 150 and 200 m/s) have been chosen for the bird impact. The initial position of the bird is according to [8] x = 4.352, y = -7.650, z = 2.430. For the impact of the bird model on the HTP structure, contact type 34 has been chosen in [8]. This contact type can be transferred to contact type NODES_TO_SURFACE in LS-DYNA, but due to high element distortion at the final end of the bird strike the contact type SURFACE_TO_SURFACE is recommended and used instead. Five integration points across the shell thickness of the leading edge were used in order to capture the onset of yielding properly.

Figure 10a depicts the artificial bird model in its initial position, while Figure 10b shows an intermediate deformation state (initial velocity 200 m/s). For the solid elements in the bird huge element distortion is well observed, leading to the desire of using an ALE- or SPH-approach to overcome this problem. Moreover high element distortion might introduce an artificial stiffening effect into the bird structure, which might in fact lead to a more localized failure and an overall to stiff behavior of the bird.

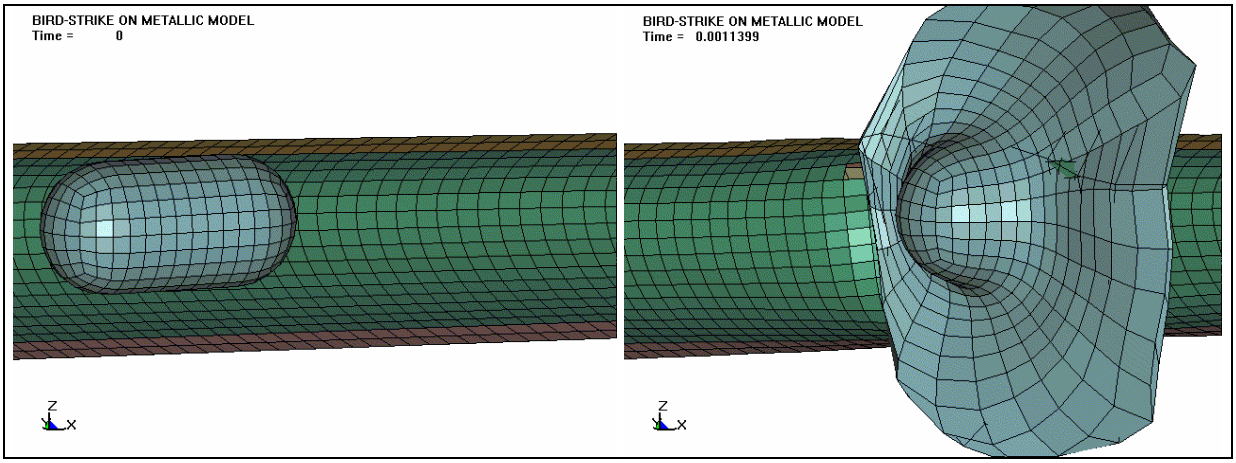

Figure 10: Bird strike (Lagrangian formulation) on metallic model

Figure 11 depicts deformation and plastic strain in case of a failure strain of 0.09. It is not only failure and rupture of the LE nose (110010) but also failure of the LE spar (110020) observed. Picture on the left side of Figure 11 correspond to time 0.00147 ms, which correlates to the normalized time t_n=1.29 in Deliverable D3.1.5 [8]. The distribution of failure qualitatively compares well with those of [8], where also failure of the LE spar was observed.

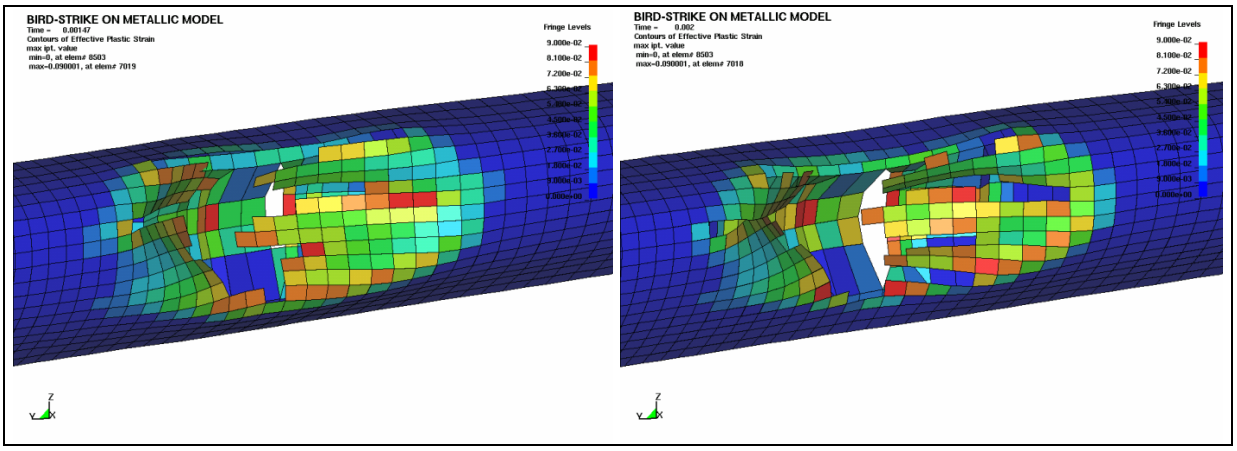

Figure 11: Failure of material parts 110010 and 110020; failure strain 0.09

Failure of the LE nose (110010) is localized and occurs only in a small region near the initial impact position. Consequently the plastic strain distribution is also localized in the impacted area. The overall movement of the HTP remains almost unchanged due to the bird strike, that means a reduced simulation model could be used as well in order to save computational costs.

Figure 12 compares the LS-DYNA results with those of National Aerospace Laboratory NLR bird strike in Deliverable 3.1.5 [8]. Deformation and failure pattern are quite similar as well as the plastic strain distribution.

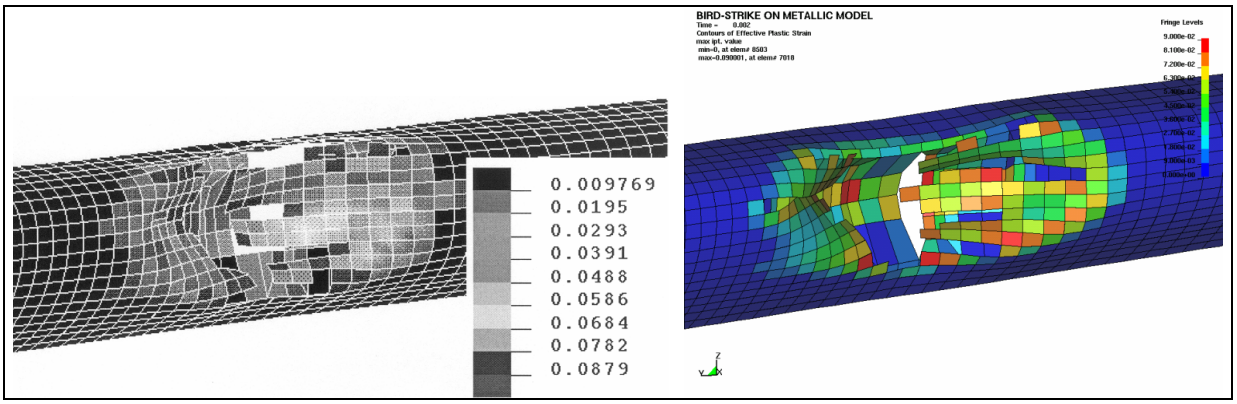

Figure 12: Comparison with National Aerospace Laboratory NLR result (D3.1.5 [8])

Bird strike (ALE formulation) on metallic HTP model

In the Lagrangian bird strike simulation of the metallic HTP it is observed, that the overall movement of the HTP is not at all influenced by the bird strike, i.e. the resultant velocity of the HTP remains unchanged. Consequently for the simulation of bird strike with the Arbitrary-Lagrangian-Eulerian (ALE) formulation a reduced model of the metallic HTP is used. Having no loss in accuracy, this will shorten computation time significantly.

Figure 13a shows the reduced HTP model for bird strike within the ALE formulation. Only the front part of the HTP in the refined region was taken and described with finite elements based on Lagrangian formulation. Nodes on the boundaries to those parts being removed have been fixed in space in order to represent the effect of the removed parts. Additionally an ALE mesh for the bird and the surrounding air (control volume) was introduced. This ALE-mesh has to be fine enough to capture the material flow of the bird through the elements properly, see Figure 13b.

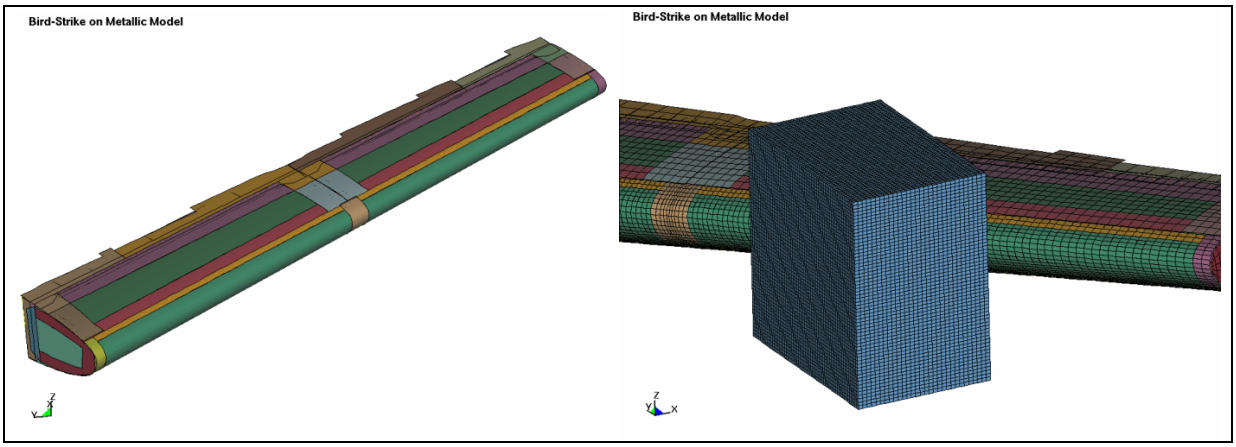

Figure 13: Reduced model for bird strike (ALE formulation) and ALE discretization

The bird within the ALE control volume has been modeled using multi-material ALE elements in combination with a multi-material group definition and an initial volume fraction definition, see Table 2. The geometry of the initial volume fraction is defined by a part, which is composed of shell elements describing the outer surface of the original bird. The initial volume fraction definition leads to an initial density distribution of the bird material inside those shell elements and the ALE mesh. It therefore describes the structure of the bird.

```
*ALE_MULTI-MATERIAL_GROUP
$      pid    idtype
  55420419         1
*ALE_MULTI-MATERIAL_GROUP
$      pid    idtype
  55420416         1
*INITIAL_VOLUME_FRACTION_GEOMETRY
$  sid_ale    st_ale     group
  55420419         1         1
$  geotype    in-out   gr-fill
         1         1         2
$      sid    sstype      iopt
  55420421         1         0
```

Table 2: Multi-material ALE in combination with initial volume fraction

Figure 14 depicts the iso-surfaces of the density distribution for the bird. An increment of two was used in the range in order to plot the bird in a sharp fashion.

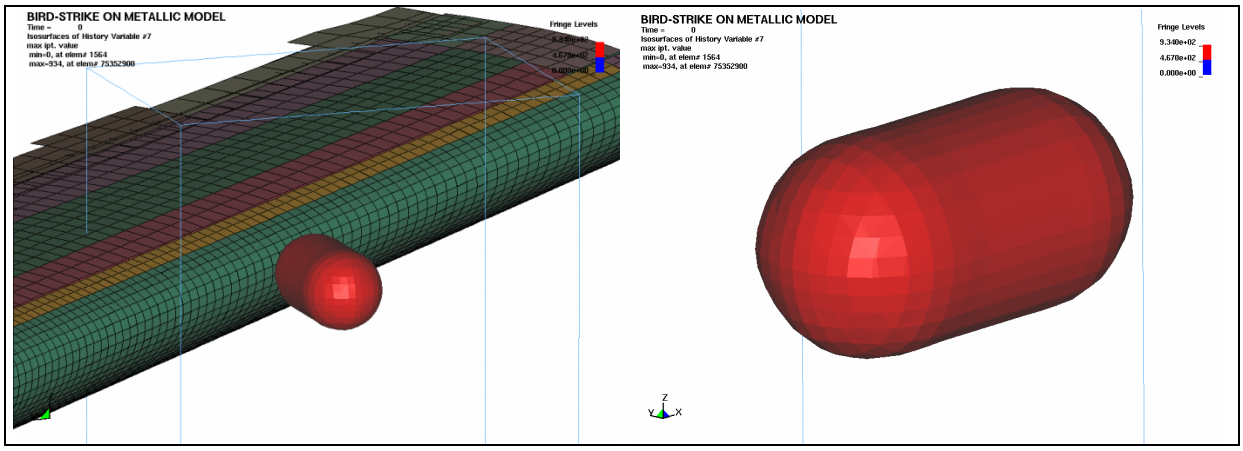

Figure 14: Bird model in ALE mesh

Contact of the bird material with the lagrange structure in form of the HTP has been defined with the *CONSTRAINED_LAGRANGE_IN_SOLID command of LS-DYNA, which basically introduces a fluid-structure-interaction coupling of bird material and lagrange structure, see **Table 3. On the** slave side the lagrangian parts are given, whereas on the master side the parts of the ALE mesh must be given. For a detailed description of the *CONSTRAINED_LAGRANGE_IN_SOLID command as well as other commands related to bird strike within ALE formulation, see [11].

```
*CONSTRAINED_LAGRANGE_IN_SOLID
$     slave     master      sstyp      mstyp      nquad      ctype      direc      mcoup
      50001      50000          0          0          4          4          2          1
$     start        end       pfac       fric     frcmin       norm     pnorm       damp
        0.0        0.0   0.800000        0.0   0.050000
$        cq       hmin       hmax      ileak      pleak    lcidpor
        0.0        0.0        0.0          0        0.0
$
*SET_PART_LIST
      50000        0.0        0.0        0.0        0.0
  55420419   55420416
*SET_PART_LIST
      50001        0.0        0.0        0.0        0.0
110010,110014,110015,1200225,1200205,110020,110018,110019
1200202,1200222,110023
```

Table 3: Contact definition of bird material with lagrange structure

For the bird material the same material as described in the previous section is used, i.e. an elasto-plastic hydrodynamic solid material in combination with a linear polynomial equation of state, see Table 1.

Figure 15 shows the bird impact on the reduced metallic HTP model. One can observe the spalling and splitting of the bird leading to fragments of the bird moving around. Compared to the Lagrangian bird strike results (Figure 11) the deformation of the leading edge is less localized but more distributed especially in the lower part of the leading edge (110010). It seems

that the ALE-formulation is softer and therefore deformation less localized. Rupture of the LE is observed as well; yet no failure occurred in the LE spar (110020), see Figure 16.

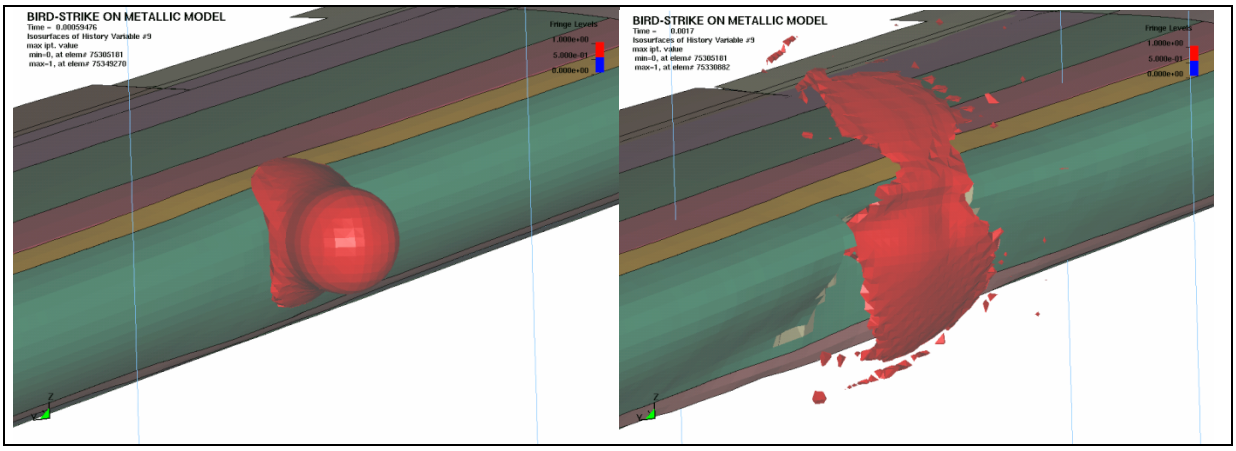

Figure 15: Bird strike (ALE formulation) on metallic model

Figure 16 shows the deformed HTP as well as the plastic strain distribution at time t_n=1.29 ms in order to obtain comparable results with the previous simulation and Deliverable D3.1.5 [8]. Similar to the indentation of the leading edge (110010) the plastic strain distribution is also less localized but eventually more spread.

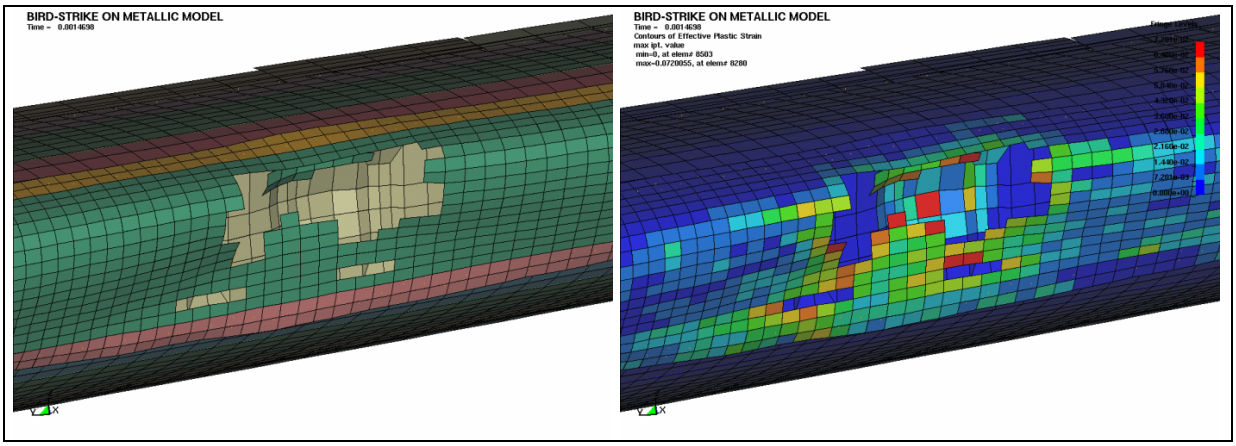

Figure 16: Deformed geometry and plastic strain distribution at time t_n=1.29

Optimization in Case of Bird Strike Using LS-OPT and LS-DYNA

Introduction into LS-OPT

For a detailed description of theory and use of LS-OPT the reader is referred to [10].

Objectives, Design Variables, Responses and Constraints

For an optimization problem it is necessary to define objectives, design variables, responses and constraints properly, i.e. in accordance and in relation to the optimization goal. Most critically in the bird strike problem is rupture and failure of the leading edge nose (110010). In that case, fragments of the bird might impact structural parts underneath or behind the leading edge eventually leading to a more severe failure. Consequently it seems to be most important that the leading edge nose does not fail respectively rupture in case of bird strike. Clearly this can be achieved by increasing the thickness of the leading edge up to a certain value. But beside that it is also important that the mass increase of the leading edge due to the non-rupture criterion is not too large. An optimum of the leading edge thickness must be found that guarantees the structural integrity and minimizes the additional mass.

Therefore the optimization problem can be formulated as follows: *Determine the thickness of the leading edge metal sheet, which minimizes the mass taking into account failure constraints in form of plastic strain at selected integration points and an additional mass constraint on the leading edge with upper and lower bounds.*

The thickness of the leading edge nose (110010) is an obvious and reasonable design variable. It was chosen with an initial value of 0.0032 m, while the design space has an upper bound of 0.006 m and a lower bound of 0.002 m. The region of interest has an initial range of 0.002 m, see Table 4.

```
variables 1
 Variable 't_110010' 0.0032
  Lower bound variable 't_110010' 0.002
  Upper bound variable 't_110010' 0.006
  Range 't_110010' 0.002
```

Table 4: Definition of the optimization problem; design variable ‘t_110010’

A quadratic polynomial approximation for the sequential Response Surface Methodology (RSM) was used in combination with a D-optimal design for the experiments. Five experiments were conducted and four iterations have been accomplished, see Table 5. The LS-DYNA runs have been done in parallel on two processors specifying the executable and the input file. Tolerances for both the design change and the objective function change have been set. Both termination criterions have been combined with the ‘and’ option, meaning that both criterions have to be fulfilled for an earlier termination.

```
Optimization Method SRSM

$
 solver dyna960 'ans1'
  solver command "/lstc/ls970/ls970_s_3535_linux_71_p"
  solver input file "/home/us/lsopt/crahvi/opt5/opt_bird_lag.k"
  solver order quadratic
  solver experiment design dopt
  solver number experiments 5
  solver basis experiment 5toK
  solver concurrent jobs 2
$
 iterate param design 0.01
 iterate param objective 0.01
 iterate param stoppingtype and
 iterate 4
STOP
```

Table 5: Definition of the optimization problem; optimization method

In total 79 responses have been defined for the bird strike problem. The purpose of responses is to monitor the history of specific values in the structure in order to be able to apply constraints onto the monitored values. The main constraints in case of bird strike seems to be a non-ruptured leading edge, i.e. part 110010 is supposed to have plastic deformations below its failure strain. Consequently for those elements being in the impact region of the bird strike the plastic strain of selected integration points across the shell thickness has been monitored and the maximum value throughout the complete time history is filtered out, see Table 6. The topmost and the bottommost integration point has been defined as response, since mainly bending is involved in case of bird strike and consequently the outermost integration points are mainly 'loaded'. Additional responses have been defined for the maximum resultant contact force, the total mass of the leading edge (110010) and the maximum of the internal energy.

```
responses 79
 response 'Internal_Energy' 1 0 "BinoutResponse -res_type GLStat -cmp
internal_energy -id 0 -select MAX"
 response 'RCFORC' 1 0 "DynaASCII RCForc R_FORCE 52 MAX"
 response 'Mass' 1 0 "DynaMass 110010 MASS"
 response 'Pl_Strain1' 1 0 "DynaASCII Elout P_STRAIN 10799 2 MAX"
 response 'Pl_Strain2' 1 0 "DynaASCII Elout P_STRAIN 10799 5 MAX"
...
```

Table 6: Definition of the optimization problem; responses

The minimization of the mass has been chosen as the objective (Table 7), since minimal mass increase is an important factor for air plane design. Moreover the minimization of the mass is up to a certain point correlated with the maximization of internal energy, which can be also regarded as dissipated energy. In any impact situation it is useful to have a maximum in dissipated energy.

```
objectives 1
 minimize
 objective 'Mass' 1
```

Table 7: Definition of the optimization problem; objective

As already mentioned constraints can be applied to those values, which have been defined as responses (see Table 6) or as design variables. In total 77 constraints have been applied. While for the mass an upper and lower bound of 15 respectively 8 was chosen, only an upper bound of 0.090 has been used for the plastic strain, see Table 8. This upper bound of the plastic strain will guarantee no rupture of the optimized leading edge, since equivalent plastic strain at failure is about 0.1.

```
constraints 77
constraint 'Mass'
 lower bound constraint 'Mass' 8
 upper bound constraint 'Mass' 15
constraint 'Pl_Strain1'
 upper bound constraint 'Pl_Strain1' 0.090
constraint 'Pl_Strain2'
 upper bound constraint 'Pl_Strain2' 0.090
constraint 'Pl_Strain11'
 upper bound constraint 'Pl_Strain11' 0.090
...
```

Table 8: Definition of the optimization problem; constraints

The input file for LS-DYNA has to be modified as well, but only minor changes are needed. Only the changes given in Table 9 are necessary in order to optimize the shell thickness of the leading edge (110010). The actual thickness of the shell is parameterized with the design variable <<t_110010>>.

```
$
*PART
$# title
Material   110010 LE-nose  h=3; Ti 6Al 4V
$#     pid     secid       mid     eosid      hgid      grav    adpopt      tmid
    110010    110010    110010         0    110010
*SECTION_SHELL
$#   secid    elform      shrf       nip     propt   qr/irid     icomp     setyp
    110010        16       0.0         5         0       0.0
$#      t1        t2        t3        t4      nloc     marea
<<t_110010>>,<<t_110010>>,<<t_110010>>,<<t_110010>>         0       0.0
$
...
```

Table 9: Minor changes in the input file for optimization of shell thickness

Figure 17a depicts the optimization history of the design variable shell thickness t_110010 in red and as thicker line in the middle, respectively. Starting from an initial value of 3.2 mm the thickness is increased to 3.63 mm at iteration four. This corresponds to a thickness change of approximately 13.4 %. Compared to the original thickness of the leading edge, which was 3 mm, this is a thickness increase of 21.0 %. The blue lines respectively outermost lines depict the size of the region of interest, which was initially chosen with 2 mm width and narrows from iteration to iteration. One may observe here the effect of the successive RSM, the panning and zooming of the region of interest. Due to the insignificant change in thickness from iteration 3 to 4 one may state, that a converged optimized solution has been found.

In Figure 17b the optimization history of the leading edge mass (110010) is shown. Starting from an initial value of 10.96 the mass increases steadily to a value of 13.12 at iteration 3. Thereafter a reduction of the mass to a value of 12.43 is again observed. The original structure had a mass of 10.27 such that a total mass increase of 21 % for the LE mass arose due to optimization. Again, the insignificant change in mass from iteration 3 to 4 is an indicator for a converged optimized solution.

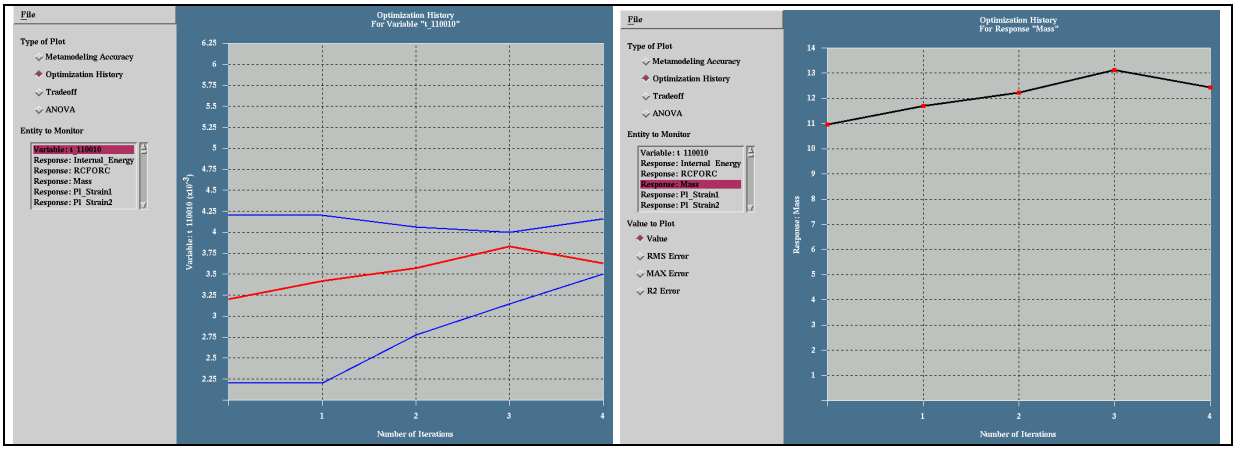

Figure 17: Optimization history of LE thickness and LE mass

Figure 18a and b depict the metamodelling accuracy for the response function ‘Internal Energy’ and ‘Pl_Strain151’, respectively. Hereby the results from the experimental design points of all iterations are depicted by squares in a coordinate system, where the horizontal axis is given by the predicted values of the approximation and the vertical axis by the computed values.

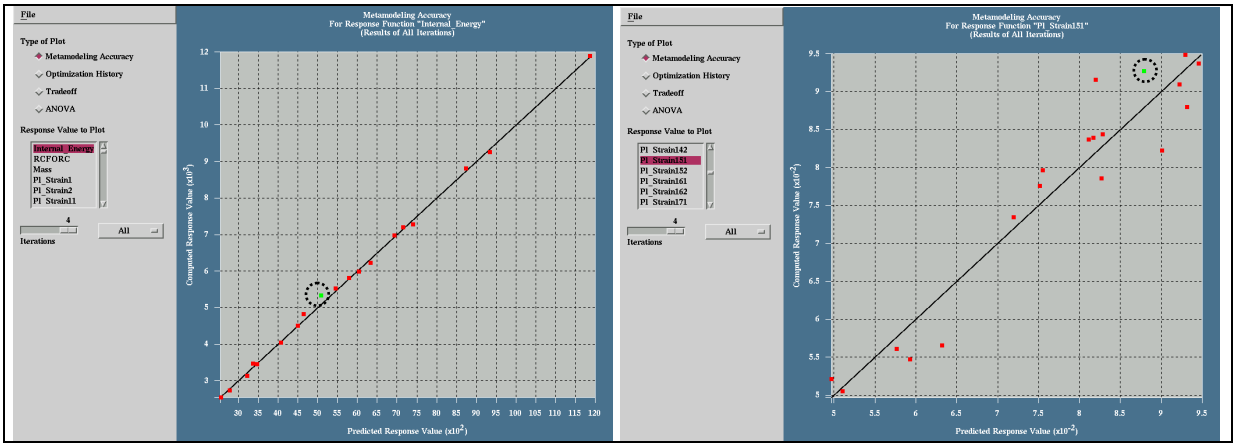

Figure 18: Metamodelling accuracy for response function ‘Internal Energy’ and ‘Pl_Strain151’

Perfect accuracy would lead to experimental design result points, which are directly lying on the bisecting line (black in Figure 18). This means, the smaller the scatter of the points, the higher the accuracy for the given response function is. In case of the response function ‘Internal Energy’ the accuracy is more than sufficient, since almost no scatter is present. The response function ‘Pl_Strain151’ corresponds to the integration point with the highest plastic strain in the

optimized structure. The accuracy for this response function is still sufficient; only minimal scattering is observed. The dashed circle marks the result point of the optimized structure.

An additional point for checking the quality of the response surface approximation is to exploit specific error norms of the response functions. The R^2-error, which varies between 0 and 1, represents the ability of the response surface to identify the variability of the design response. A low value of R^2 usually means that the region of interest is either too large or too small and that the gradients are not trustworthy. The value of 1.0 for R^2 indicates a perfect fit. However the value will not warn against an over fitted model with poor prediction capacities [10]. Figure 19 depicts the R2-error norms of response 'Mass' and 'Pl_Strain151'. In case of 'Mass' response a horizontal line at 1.0 is observed.

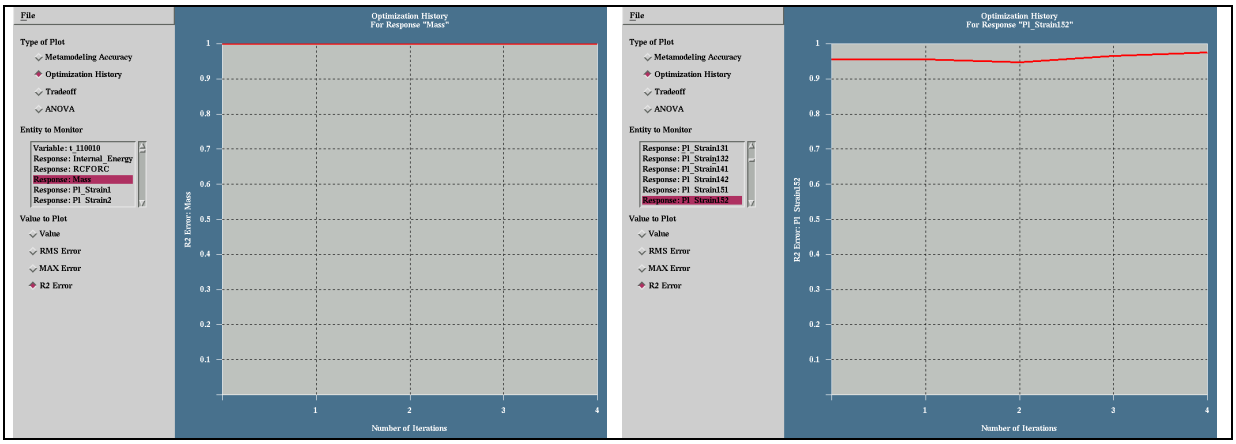

Figure 19: R^2-error for response 'Mass' and 'Pl_Strain151'

Figure 20a depicts the deformation of the optimized structure. First of all, one may observe that no failure of the leading edge nose occurred, that means it is unruptured due to the higher thickness. The deformation is more distributed along the height of the leading edge. Similar to the deformation, the plastic strain distribution in Figure 20b is also less localized.

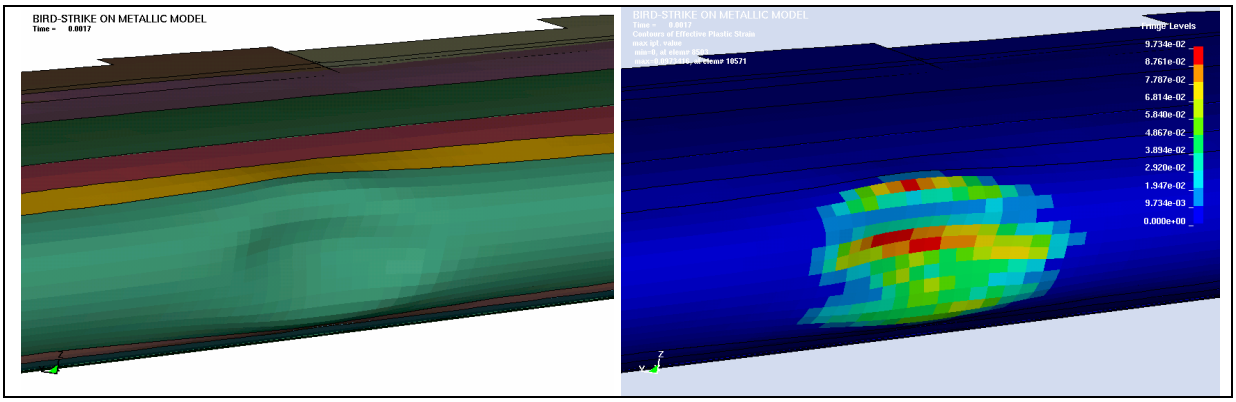

Figure 20: Deformation and plastic strain distribution of optimized leading edge (110010)

Figure 21depicts the deformation of the original and the optimized leading edge.

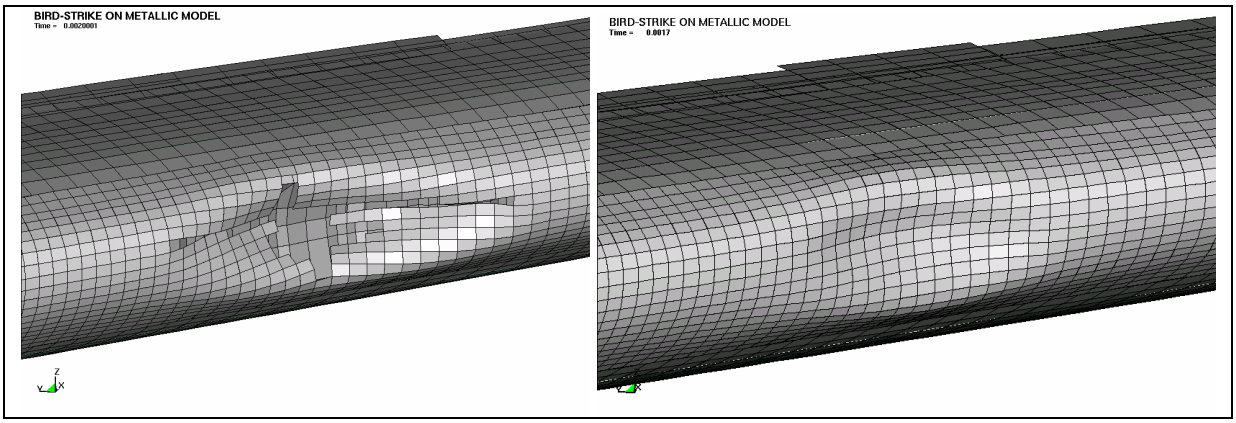

Figure 21: Deformation of original and optimized leading edge (110010)

In Figure 22 a comparison of total, kinetic, and internal energy of both the original and the optimized structure is shown. One may observe that the internal energy in the optimized structure is reduced, since the thickness of the leading edge has been increased. Consequently the stiffness of the leading edge is increased as well and deformations become smaller. Naturally less deformation energy is then obtained.

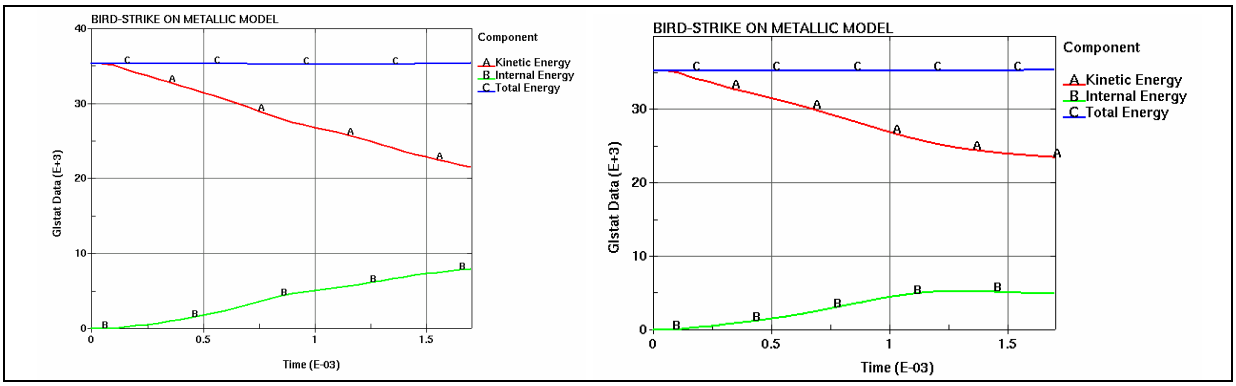

Figure 22: Energy: initial vs. optimized leading edge

Conclusion

The current contribution presented simulation results of rigid pole impact on composite HTP model, bird strike on metallic HTP model within Lagrangian as well as ALE formulation. For the rigid pole impact the obtained numerical results agree remarkable well with those available within the CRAHVI-Programme. In case of Lagrangian bird strike the results were compared with those of the National Aerospace Laboratory NLR [8]. Both deformation and failure pattern as well as the plastic strain distribution agree well. The results in case of bird strike within ALE-formulation are slightly different compared to those of the Lagrangian model. Deformation and failure pattern as well as plastic strain distribution are more spread, i.e. less localized in case of ALE formulation. Either the Lagrangian formulation is too stiff as a matter of highly distorted elements or the ALE-formulation in combination with the used material model is too soft.

Additionally optimization results of the LE obtained from LS-OPT in combination with LS-DYNA are shown, which fulfill the desired optimization criterion of a non-ruptured leading edge, i.e. the structural integrity of the HTP is not lost.

References

[1] Xiao, J.R. and McCarthy M.A., "HTP PAM-CRASH Model (refined mesh)", CRAHVI Deliverable 3.1.2, (2002).

[2] McCarthy, M.A. and Xiao J.R., "HTP PAM-CRASH Composite Model", CRAHVI Deliverable 3.1.3, (2002).

[3] McCarthy, M.A. and Xiao J.R., "HTP PAM-CRASH Composite Model, Addendum to 3.1.3", CRAHVI Deliverable D3.1.3a, (2002).

[4] Sunaric, M. and Kermanidis T., "HTP PAM-CRASH Metallic Model", CRAHVI Deliverable 3.1.4, (2002).

[5] McCarthy, M.A. and Xiao J.R., "Deterministic PAM-CRASH Models and Reference Shots for Obstacle Impact with HTP in Survivable Crash Scenarios", CRAHVI Deliverable 3.1.7, (2002).

[6] Brown, T., "Lagrangian bird model", CRAHVI Deliverable 1.4.3, (2002).

[7] Johnson, A. and Holzapfel, M., "Modelling of bird strike on a rigid wall and metal panel", DLR report IB-435-2001/19, (2001).

[8] van Houten, M.H., "Bird strike on HTP: reference shots", CRAHVI Deliverable 3.1.5, (2002).

[9] Bergler, Ch., Kracht, M. and Rust, W., "HTP-Reference Metallic and Composite Deterministic Shots with LS-DYNA", CRAHVI Deliverable 3.1.9, (2202).

[10] Stander, N et al., "Design Optimization Software for the Engineering Analyst", LS-OPT User's Manual, Livermore Software Technology Corporation, (2003).

[11] Livermore Software Technology Corporation, "LS-DYNA Keyword User's Manual", (2003).